Thermodynamically consistent hydrodynamic computational models for high-Knudsen-number gas flows

R. S. Myong[a)]
NASA Goddard Space Flight Center, Mail Stop 930, Greenbelt, Maryland 20771

(Received 4 November 1998; accepted 2 June 1999)

In high-Knudsen-number flows nonequilibrium effects become dominant and the use of Navier–Stokes–Fourier equations becomes questionable since they are based on small deviation from local thermodynamic equilibrium. In this paper new hydrodynamic computational models are proposed for modeling gases in the transition regime. They are based on Eu's generalized hydrodynamic equations and it turns out that they apply in all Mach numbers and satisfy the second law of thermodynamics to every order of approximation. In order to learn more about the new equations a model equation similar to the Burgers' equation is studied. From this analysis new insight into constitutive relations of various hydrodynamic equations has been gained. In addition, a convergent iterative method for solving the highly nonlinear constitutive equations is developed. Finally, the shock structure and slip flow problems are computed by using high resolution numerical schemes and issues of extending the one-dimensional solver to multidimensional problems are discussed.
 [S1070-6631(99)02909-8]

I. INTRODUCTION

Fluid dynamical descriptions of gases are based on the continuum assumption that the mean free path of a particle is much smaller than the characteristic lengths of interest. This assumption enables us to describe the motion of gases by some measurable macroscopic quantities, e.g., density, velocity, and temperature. Fluid dynamic equations can be represented by hyperbolic conservation laws on conserved variables (density, momentum, energy) and an equation of state that characterizes the properties of gases. In addition to an equation of state, to obtain a complete mathematical description the conservation laws must be supplemented by the constitutive relations between conserved variables and measurable, but nonconserved variables (stress and heat flux). Even though both the equation of state and the constitutive relations play a very important role in determining the structure of flows in gases, the constitutive relations provide a more challenging mathematical problem. The main reason is that they intend to explain phenomena which couple distinct length or time scales and such a multiscale feature can cause more difficulty as the basic assumption deviates from the continuum assumption. It often becomes a daunting task to model gases in the transition regime that lies between free molecular flow and continuum flow.

This situation is not confined to rare problems of engineering and scientific interest. Indeed, there exist many needs for rapid exploitation of new technologies. For example, the prediction of aerothermodynamic loads on vehicles that operate in high altitude requires the knowledge of rarefied gas dynamics (RGD).[1] In this case, the low density is the source of high-Knudsen-number effect which measures the deviation from the continuum description. Another example is gas flows in microscale channels of microelectromechanical systems (MEMS).[2,3] Since the microscale flow usually occurs in an atmospheric condition, small scale is the cause of deviation. Furthermore, it should be mentioned that the low density and microscale flows can occur in conjunction with nearly continuum flows. In hypersonic vehicles, the localized low density regime can be found near the leading edge. In this case, continuum and transition regimes coexist and consequently the computation becomes very demanding. For the same reason, the microscale effect may become important in exploring the transition, which is closely related to turbulence, near the solid wall. The study of the transition might require microscale physics, becoming the multiscale science. All these problems contribute to making the study of high-Knudsen-number flow very challenging.

Previous efforts have employed fluid dynamics and the full kinetic model in either an uncoupled or coupled (hybrid) way. At low enough densities, the direct simulation Monte Carlo (DSMC) method[4,5] has been used to solve the kinetic model. Currently, it is the most reliable and widespread method for the computation of high-Knudsen-number flow. However, since the fundamental idea is based on tracking a large number of statistically representative particles, the computational cost can be prohibitive in regimes near continuum limit. Even in regimes away from such limit, the computation by DSMC can be far beyond the current computing capability. For instance, such a case occurs in microscale flow[6] owing to the relatively high density and low velocity. On the other hand, the fluid dynamic model is based on the hyperbolic conservation laws of collision-free conserved variables. The stress tensor and heat flux appearing in the conservation laws are calculated by the constitutive relations that express the stress and heat flux in terms of con-

[a)]Present address: Division of Aerospace and Mechanical Engineering, Gyeongsang National University, Chinju, Gyeongnam 660-701, Republic of Korea; electronic mail: myong@nongae.gsnu.ac.kr

served variables and their derivatives. Higher-order terms that may exist in the constitutive relations can be removed by the next level of constitutive relations. In this formulation it is the constitutive relations that determine the accuracy of approximate hydrodynamic models. One of these models is the Burnett equations, which use the Chapman–Enskog expansion to derive higher-order terms.[7–9] They are intended to describe second-order departures from thermal equilibrium and were used extensively to simulate the hypersonic flow in transition regimes. It was shown, however, that because of the presence of higher derivative terms, an additional boundary condition is needed for the solutions to be uniquely determined, and different solutions can result from the choice of the boundary values.[10] It is also known that some of the Burnett equations developed by far can violate the second law of thermodynamics at very high Knudsen numbers and some flow conditions.[11,12] Another hydrodynamic model is the moment method which works with the equations of transfers instead of dealing with the distribution function.[13,14,7,15] In the moment method the distribution function is expanded in moments and the evolution equations for moments are derived from the Boltzmann equation. In principle, this method might lead to a set of macroscopic equations consistent with the second law of thermodynamics, but most of the methods, e.g., Grad's 13 moment method, result in the entropy balance equation being inconsistent with the Gibbs relation.[16,17] This shortcoming was dealt with by recent work on the so-called Gaussian closure.[18,19] This closure is based on a more elegant choice of a finite-dimensional linear subspace and yields a hyperbolic moment system. Since the hyperbolicity is easier to implement numerically, Groth *et al.*[20] developed some computational models based on this closure. However, it turns out that the Gaussian closure is of limited practical interest, since the primary system with 10 variables admits no heat flux and the other systems, e.g., the 35 moment system, do not yield numerical solutions above Mach numbers of approximately two.[21]

For a lack of reliable high-order fluid dynamic models and the limits of computing power, it becomes fashionable to employ a hybrid approach which couples an Euler or Navier–Stokes solver with DSMC. It is possible that this approach can provide some benefits since it takes advantage of good properties of each method. The hybrid codes can be developed for problems that contain disconnected nonequilibrium regions embedded in a continuum flow.[5,22] However, the development of such a method is not trivial since two issues have to be solved before implementation; (1) when to switch between the two methods and (2) how to pass information from one method to another.[23] Furthermore, conceptual inconsistency still remains since fluid dynamic equations have to recover both free-molecular and Navier–Stokes (continuum) limits. The recovery of only one limit may not be enough to combine with DSMC.

In this study, important factors are discussed which have to be taken into account in developing extended hydrodynamic models. As a result, distinct computational models are proposed which provide not only accurate predictions, but also fill the gap between kinetic and continuum approaches. The present study is based on the pioneering work of generalized hydrodynamics (GH) by Eu.[24,25] It is Eu's evolution equations within the framework of 13 moments that provide the basis of our computational models. From the early 1980s, Eu has developed a method of solving the Boltzmann equation, especially with a view to a deeper understanding of irreversible thermodynamics for systems in a nonequilibrium state. According to his argument, the second law of thermodynamics should be satisfied to every order of approximation or by whatever approximation made to the distribution function. From his point of view, a number of problems residing in previous hydrodynamic models arise from not taking into account the entropy in the solution method. His works of irreversible thermodynamics were published largely in the chemistry community and consequently their importance has not been fully recognized in other communities. Here the advantages of this method are identified and then thermodynamically consistent computational models for modern computational fluid dynamics (CFD) codes are developed. The main focus is to develop efficient computational models which can serve as the basic building blocks to problems in higher space dimensions. Important practical benefits can be gained by being equipped with (1) an engineering tool for designing and modeling an aerospace vehicle in a high-altitude region and MEMS, (2) proper hydrodynamic models for hybrid fluid/kinetic simulations, (3) an analysis tool for the study of turbulence based on a hydrodynamic model which has a better capability of incorporating microscopic behavior.

This paper is organized as follows. In Sec. II various aspects of developing computational models for high-Knudsen-number flows are discussed. From Eu's original generalized hydrodynamic equations, distinct computational models adequate to modern CFD codes are derived. In Sec. III, by studying a model equation, namely, the GH-Burgers equation, new insight into the constitutive relations of various hydrodynamic equations including the new model is gained. In Secs. IV and V one-dimensional thermodynamically consistent computational models for high-Knudsen-number flows are presented. In addition, numerical methods that will be used to solve the hydrodynamic equations are described and some numerical results for shock-structure and slip-velocity problems are also given. In Secs. VI and VII issues of further development are discussed. In the Appendices, a summary of the new idea of Eu's generalized hydrodynamics is included.

II. GENERALIZED HYDRODYNAMIC COMPUTATIONAL MODELS

It is well known that the role of thermodynamics becomes important in nonequilibrium flows. Thus it may be critical to ensure that thermodynamics is properly incorporated into the derivation of hydrodynamic equations from the Boltzmann equation. Recently, the generalized hydrodynamic equations based on a nonequilibrium canonical distribution function and a cumulant expansion of the collisional integral were developed by Eu.[25,26] They can be regarded as a thermodynamically consistent macroscopic equation. It also turns out that they recover the correct behavior at con-

tinuum and free molecular limits. The main feature of the generalized hydrodynamic equations is summarized in the Appendices A–C.

If the system consists of a single-component monatomic gas, the evolution equations in the spirit of 13 moments can be written as[25]

$$\begin{pmatrix} \rho \\ \rho \mathbf{u} \\ \rho E \end{pmatrix}_t + \boldsymbol{\nabla} \cdot \begin{pmatrix} \rho \mathbf{u} \\ \rho \mathbf{u}\mathbf{u} + p\mathbf{I} \\ (\rho E + p)\mathbf{u} \end{pmatrix} + \boldsymbol{\nabla} \cdot \begin{pmatrix} 0 \\ \boldsymbol{\Pi} \\ \boldsymbol{\Pi} \cdot \mathbf{u} + \mathbf{Q} \end{pmatrix} = 0, \tag{1}$$

and

$$\rho \frac{D(\boldsymbol{\Pi}/\rho)}{Dt} = -\boldsymbol{\nabla} \cdot \psi_2 - 2[\boldsymbol{\Pi} \cdot \boldsymbol{\nabla} \mathbf{u}]^{(2)} - \frac{p}{\eta}\{\boldsymbol{\Pi} q(\kappa) + 2\eta[\boldsymbol{\nabla} \mathbf{u}]^{(2)}\}, \tag{2}$$

$$\rho \frac{D(\mathbf{Q}/\rho)}{Dt} = -\boldsymbol{\nabla} \cdot \psi_3 - \boldsymbol{\Pi} \cdot C_p \boldsymbol{\nabla} T + \boldsymbol{\nabla} \cdot (p\mathbf{I} + \boldsymbol{\Pi}) \cdot \frac{\boldsymbol{\Pi}}{\rho} - \mathbf{Q} \cdot \boldsymbol{\nabla} \mathbf{u} - \frac{pC_p T}{\lambda}\{\mathbf{Q} q(\kappa) + \lambda \boldsymbol{\nabla} \ln T\} \tag{3}$$

where

$$q(\kappa) = \frac{\sinh(\kappa)}{\kappa} \tag{4}$$

and

$$\kappa = \frac{(mk_B)^{1/4}}{\sqrt{2}d} \frac{T^{1/4}}{p} \left[\frac{\boldsymbol{\Pi} : \boldsymbol{\Pi}}{2\eta} + \frac{\mathbf{Q} \cdot \mathbf{Q}}{\lambda} \right]^{1/2}. \tag{5}$$

Here ρ is the mass density, $\mathbf{u}$ is the fluid velocity, p is the pressure, T is the temperature, E is the total energy density, Π is the shear stress, and $\mathbf{Q}$ is the heat flux. A derivative D/Dt represents the substantial derivative. The C_p is the heat capacity per mass at constant pressure. The symbol $[\nabla \mathbf{u}]^{(2)}$ stands for the traceless symmetric part of $\nabla \mathbf{u}$ and its k, ℓ components can be expressed in tensor notation

$$[\boldsymbol{\nabla} \mathbf{u}]^{(2)} = \frac{1}{2}\left(\frac{\partial u_k}{\partial x_\ell} + \frac{\partial u_\ell}{\partial x_k} \right) - \frac{1}{3} \delta_{k\ell} \frac{\partial u_i}{\partial x_i}, \quad i = 1,2,3,$$

where $\delta_{k\ell}$ denotes the unit second-rank tensor. The term $[\Pi \cdot \nabla \mathbf{u}]^{(2)}$ represents the coupling between the shear stress and velocity gradient and its k, ℓ components are

$$[\boldsymbol{\Pi} \cdot \boldsymbol{\nabla} \mathbf{u}]^{(2)} = \frac{1}{2}\left(\Pi_{ik} \frac{\partial u_\ell}{\partial x_i} + \Pi_{i\ell} \frac{\partial u_k}{\partial x_i} \right) - \frac{1}{3} \delta_{k\ell} \Pi_{ij} \frac{\partial u_i}{\partial x_j}, \quad i,j = 1,2,3.$$

The ψ_2 and ψ_3 are higher-order moments. The η and λ are the Chapman–Enskog viscosity and thermal conductivity, respectively. These coefficients can be dense-gas material functions, so that the evolution equations can be applied to dense gases. The κ is the first-order cumulant of cumulant approximation for dissipation terms; d denotes the diameter of the molecule and depends only on T; m is the molecular mass; and k_B is the Boltzmann constant. The colon in κ denotes the double scalar product between tensors.

The unique feature of the constitutive relations can be found in a nonlinear factor $q(\kappa)$ in the last terms. The role of $q(\kappa)$ can be manifested when entropy production is considered. The entropy production for generalized hydrodynamics, which measures energy dissipation arising from molecular collisions, can be expressed in a reduced form

$$\sigma^*_{\text{ent}} = \sigma_{\text{ent}} G/k_B = \kappa^2 q(\kappa), \tag{6}$$

where $G = (m/k_B T)^{1/2}/(2n^2 d^2)$. n is the number density. Obviously,

$$\sigma_{\text{ent}} \geqslant 0, \tag{7}$$

which means that generalized hydrodynamics satisfies the second law of thermodynamics.

Before we examine the new equations in detail, let us make them dimensionless. Let us first introduce the parameters

$$t^* = t/(L/u_r), \quad \mathbf{x}^* = \mathbf{x}/L, \quad \eta^* = \eta/\eta_r,$$
$$\lambda^* = \lambda/\lambda_r, \quad \mathbf{u}^* = \mathbf{u}/u_r, \quad \rho^* = \rho/\rho_r, \quad T^* = T/T_r,$$
$$p^* = p/p_r, \quad C_p^* = C_p/C_{pr}, \quad E^* = E/u_r^2,$$
$$\boldsymbol{\Pi}^* = \boldsymbol{\Pi}/(\eta_r u_r/L), \quad \mathbf{Q}^* = \mathbf{Q}/(\lambda_r \Delta T/LT_r),$$

where the subscript r represents the reference state. Here L denotes the characteristic length, ΔT denotes $T_w - T_r$ or $T_r - T_w$ where T_w is the wall temperature. Then some dimensionless numbers, Mach (M), Reynolds (Re), Eckert (Ec), Prandtl (Pr), can be defined:

$$M \equiv \frac{u_r}{a_r} = \frac{u_r}{(\gamma R T_r)^{1/2}}, \quad \text{Re} \equiv \frac{\rho_r u_r L}{\eta_r},$$
$$\text{Ec} \equiv \frac{u_r^2}{C_{pr} \Delta T}, \quad \text{Pr} \equiv \frac{C_{pr} \eta_r}{\lambda_r / T_r}, \tag{8}$$

where a is the speed of sound and R is a gas constant. It follows that

$$N_\delta \equiv \frac{\eta_r u_r}{p_r L} = \frac{\gamma M^2}{\text{Re}}, \tag{9}$$

where γ is the specific heat ratio. This composite number introduced by Eu, which measures the magnitude of the viscous stress relative to the hydrostatic pressure, indicates the level of departure from equilibrium and is particularly useful in the study of high-Knudsen-number flow. If the mean free path is given by $l = (\pi/2)^{1/2} \eta_r (RT_r)^{-1/2}/\rho_r$, the Knudsen number can be expressed as

$$\text{Kn} \equiv \frac{l}{L} = \sqrt{\frac{\gamma \pi}{2}} \frac{M}{\text{Re}} = \sqrt{\frac{\pi}{2\gamma}} \frac{N_\delta}{M}. \tag{10}$$

It should be noted that Ec and $\mathbf{Q}^*$ reduce to $u_r^2/C_{pr}T_r$ and $\mathbf{Q}/(\lambda_r/L)$, respectively, in the shock structure problem and when $T_w = T_r$. In that case, $\text{Ec} = (\gamma - 1)M^2$.

Then, if $d^* = d/d_r$, κ becomes

$$\kappa = \left(\frac{(mk_B T_r)^{1/4}}{d_r \sqrt{\eta_r}} \right) N_\delta \frac{T^{*1/4}}{2d^* \sqrt{\eta^*} p^*} [\boldsymbol{\Pi}^* : \boldsymbol{\Pi}^* + 2\epsilon(\eta^*/\lambda^*) \mathbf{Q}^* \cdot \mathbf{Q}^*]^{1/2}, \tag{11}$$

where

$$\epsilon=\frac{1}{\mathrm{Ec\,Pr}}\frac{1}{T_r/\Delta T}. \tag{12}$$

Here the factor $(mk_{\mathrm{B}}T_r)^{1/4}/d_r\eta_r^{1/2}$ can be further simplified. Note that for a simple gas (Ref. 7, p. 226)

$$\eta^*=T^{*s},\quad \frac{\eta^*}{\lambda^*}=\frac{1}{T^*},\quad d^*=T^{*1/(1-\nu)},\quad \frac{T^{*1/4}}{d^*\sqrt{\eta^*}}=1, \tag{13}$$

which follow from the formulas

$$\eta=\frac{5}{8A_2(\nu)\Gamma[4-2/(\nu-1)]}\frac{1}{d^2}\sqrt{\frac{mk_{\mathrm{B}}T}{\pi}}, \tag{14}$$

$$\lambda/T=\frac{C_p\eta}{\mathrm{Pr}}, \tag{15}$$

$$d=\left(\frac{K}{2k_{\mathrm{B}}T}\right)^{1/(\nu-1)}, \tag{16}$$

where $s=\frac{1}{2}+2/(\nu-1)$, ν is the exponent of the inverse power laws, and K is their coefficient. Then the factor $(mk_{\mathrm{B}}T_r)^{1/4}/d_r\eta_r^{1/2}$ reduces to

$$\left[\frac{8\sqrt{\pi}}{5}A_2(\nu)\Gamma[4-2/(\nu-1)]\right]^{1/2}.$$

Finally, κ becomes

$$\kappa=N_\delta\kappa^*=\frac{cN_\delta}{p^*}[\boldsymbol{\Pi}^*:\boldsymbol{\Pi}^*+\mathbf{Q}^*\cdot\mathbf{Q}^*/(T^*/2\epsilon)]^{1/2}, \tag{17}$$

where

$$c=\left[\frac{2\sqrt{\pi}}{5}A_2(\nu)\Gamma[4-2/(\nu-1)]\right]^{1/2}.$$

Only the parameters M, Re, Ec, Pr, ϵ, c, and γ appear since $N_\delta=\gamma M^2/\mathrm{Re}$. We list a few examples for intermolecular forces below.

(1) *Rigid elastic sphere* ($\nu\to\infty, s=0.5$): For a rigid elastic spherical molecule,

$$A_2(\infty)=\tfrac{1}{3},\quad \Gamma(4)=6,\quad c=1.1908. \tag{18}$$

(2) *Argon* ($\nu=9, s=0.75$): For an argon molecule,

$$A_2(9)=0.3304,\quad \Gamma(3.75)=4.423,\quad c=1.0179. \tag{19}$$

(3) *Maxwellian* ($\nu=5, s=1$): For a Maxwellian molecule,

$$A_2(5)=0.43619,\quad \Gamma(3.5)=\frac{15}{8}\sqrt{\pi},\quad c=1.0138. \tag{20}$$

Finally, if we drop the asterisks, the dimensionless evolution equations of a monatomic gas can be written as

$$\begin{pmatrix}\rho\\ \rho\mathbf{u}\\ \rho E\end{pmatrix}_t+\boldsymbol{\nabla}\cdot\begin{pmatrix}\rho\mathbf{u}\\ \rho\mathbf{u}\mathbf{u}+\frac{1}{N_\delta\mathrm{Re}}p\mathbf{I}\\ \left(\rho E+\frac{1}{N_\delta\mathrm{Re}}p\right)\mathbf{u}\end{pmatrix}+\frac{1}{\mathrm{Re}}\boldsymbol{\nabla}\cdot\begin{pmatrix}0\\ \boldsymbol{\Pi}\\ \boldsymbol{\Pi}\cdot\mathbf{u}+\frac{1}{\mathrm{Ec\,Pr}}\mathbf{Q}\end{pmatrix}=0, \tag{21}$$

and

$$\rho\frac{D(\boldsymbol{\Pi}/\rho)}{Dt}=-\boldsymbol{\nabla}\cdot\psi_2-2[\boldsymbol{\Pi}\cdot\boldsymbol{\nabla}\mathbf{u}]^{(2)}-\frac{1}{N_\delta}\frac{p}{\eta}\{\boldsymbol{\Pi}q(N_\delta\kappa)+2\eta[\boldsymbol{\nabla}\mathbf{u}]^{(2)}\}, \tag{22}$$

$$\rho\frac{D(\mathbf{Q}/\rho)}{Dt}=-\boldsymbol{\nabla}\cdot\psi_3-\mathrm{Pr}\,\boldsymbol{\Pi}\cdot C_p\boldsymbol{\nabla}T+\mathrm{Ec\,Pr}\,\boldsymbol{\nabla}\cdot\left(\frac{1}{N_\delta\mathrm{Re}}p\mathbf{I}+\frac{1}{\mathrm{Re}}\boldsymbol{\Pi}\right)\cdot\frac{\boldsymbol{\Pi}}{\rho}-\mathbf{Q}\cdot\boldsymbol{\nabla}\mathbf{u}-\frac{\mathrm{Pr}}{N_\delta}\frac{pC_pT}{\lambda}\{\mathbf{Q}q(N_\delta\kappa)+\lambda\boldsymbol{\nabla}\ln T\}, \tag{23}$$

where

$$q(N_\delta\kappa)\equiv\frac{\sinh(N_\delta\kappa)}{N_\delta\kappa}, \tag{24}$$

and

$$\kappa=\frac{c}{p}\{\boldsymbol{\Pi}:\boldsymbol{\Pi}+\mathbf{Q}\cdot\mathbf{Q}/(T/2\epsilon)\}^{1/2}. \tag{25}$$

Here it is assumed that higher-order moments ψ_2 and ψ_3 are made dimensionless. For a polytropic monatomic gas the following relations hold:

$$p=\rho T=\rho a^2,\quad \rho E=\frac{p/(N_\delta\mathrm{Re})}{(\gamma-1)}+\tfrac{1}{2}\rho\mathbf{u}\cdot\mathbf{u},\quad \gamma=\tfrac{5}{3},\quad \mathrm{Pr}=\tfrac{2}{3},\quad \eta=T^s,\quad \lambda=T^{s+1},\quad C_p=1. \tag{26}$$

Notice that the dimensionless conservation laws are somewhat different from the conventional form because of the presence of the factor $1/N_\delta\mathrm{Re}$. In order to close the constitutive relations (22) and (23) the higher-order moments ψ_2 and ψ_3 must be expressed in the lower-order moments, the nonconserved moments $\boldsymbol{\Pi}$ and $\mathbf{Q}$, as well as the conserved moments ρ, $\mathbf{u}$, and E. Here we employ Eu's closure in Appendix *B* that

$$\psi_2=\psi_3=0. \tag{27}$$

Then when Eqs. (21)–(26) are solved subject to initial and boundary conditions, their solutions will provide all the properties of the fluid undergoing irreversible processes. However, it becomes apparent that the evolution equations in the present forms are not suitable for numerical methods on hyperbolic conservation laws. The reason is that the constitutive relations are highly nonlinear and it seems impossible to recast the governing equations in the conservative form. In Secs. II A–II C we will derive several approximate constitutive relations and describe the physical reasoning behind such approximations.

A. Adiabatic approximation

By Eu's closure, Eqs. (21)–(26) become the partial differential equations of macroscopic variables $(\rho,\mathbf{u},E,\mathbf{\Pi},\mathbf{Q})$ in a function of position and time. However, it seems very difficult to deal with the partial differential equations of the constitutive relations (22) and (23), while those of collision-free variables (21) can be easily dealt with by numerical schemes on hyperbolic conservation laws. This difference may motivate an approximation by which the constitutive equations are simplified into a numerically solvable form. Such as approximation is, indeed, possible if we observe that the set of macroscopic variables consists of two subsets, the conserved set $(\rho,\mathbf{u},E)$ and the nonconserved set $(\mathbf{\Pi},\mathbf{Q})$ which vary on two different time scales. It may be estimated that the relaxation times of the nonconserved variables are very short, being of the order of 10^{-10} s. Owing to such a small time scale, on the time scale of variation in the conserved variables the nonconserved variables have already reached their steady state. Therefore, the constitutive relations can be algebraically solved with the conserved variables held constant, and they become

$$-(\mathbf{u}\cdot\nabla)\mathbf{\Pi}-\mathbf{\Pi}(\nabla\cdot\mathbf{u})-2[\mathbf{\Pi}\cdot\nabla\mathbf{u}]^{(2)} - \frac{1}{N_\delta}\frac{p}{\eta}\{\mathbf{\Pi}q(N_\delta\kappa)+2\eta[\nabla\mathbf{u}]^{(2)}\}=0, \tag{28}$$

$$-(\mathbf{u}\cdot\nabla)\mathbf{Q}-\mathbf{Q}(\nabla\cdot\mathbf{u})-\mathrm{Pr}\,\mathbf{\Pi}\cdot\nabla T+\mathrm{Ec}\,\mathrm{Pr}\,\nabla \cdot\left(\frac{1}{N_\delta\mathrm{Re}}p\mathbf{I}+\frac{1}{\mathrm{Re}}\mathbf{\Pi}\right)\cdot\frac{\mathbf{\Pi}}{\rho}-\mathbf{Q}\cdot\nabla\mathbf{u}-\frac{\mathrm{Pr}}{N_\delta}\frac{p}{\lambda/T}\{\mathbf{Q}q(N_\delta\kappa) +\lambda\nabla\ln T\}=0. \tag{29}$$

This approximation is called the adiabatic approximation and reduces numerical difficulty considerably.

B. GH computational models

The constitutive relations (28) and (29) can reduce to more manageable forms without losing the essence of their nonlinearity. An approximation can be made on the physical ground that the terms without N_δ^{-1} are neglected since they are kinematic in origin and responsible for couplings between different modes of irreversible transport. On the other hand, we keep the nonlinear factor $q(N_\delta\kappa)$ intact to retain the effect of nonlinear energy dissipation occurring through molecular collisions. The constitutive relations then become

$$\mathbf{\Pi}q(N_\delta\kappa)=\mathbf{\Pi}_0, \tag{30}$$

$$\mathbf{Q}q(N_\delta\kappa)=\mathbf{Q}_0, \tag{31}$$

where the Navier–Stokes–Fourier constitutive relations are defined as

$$\mathbf{\Pi}_0\equiv-2\eta[\nabla\mathbf{u}]^{(2)}, \tag{32}$$

$$\mathbf{Q}_0\equiv-\lambda\nabla\ln T. \tag{33}$$

The definition of heat flux is different from the well-known Fourier law, but it does not make any difference. Rather, the present one is convenient for developing irreversible thermodynamics because the present definition of the thermodynamic force corresponding to heat flow arises naturally. It must be, however, noted that λ is equal to λ (Chapman—Enskog) times T. If we take the scalar product of $\mathbf{\Pi}$ and $\mathbf{Q}$ and then add them to form κ defined in (25), we obtain

$$\kappa q(N_\delta\kappa)=\kappa_0, \tag{34}$$

where

$$\kappa_0=\frac{c}{p}\{\mathbf{\Pi}_0:\mathbf{\Pi}_0+\mathbf{Q}_0\cdot\mathbf{Q}_0/(T/2\epsilon)\}^{1/2}. \tag{35}$$

Equation (34) leads to a pair of solutions for $\mathbf{\Pi}$ and $\mathbf{Q}$,

$$\mathbf{\Pi}=\frac{\sinh^{-1}(N_\delta\kappa_0)}{N_\delta\kappa_0}\mathbf{\Pi}_0, \tag{36}$$

$$\mathbf{Q}=\frac{\sinh^{-1}(N_\delta\kappa_0)}{N_\delta\kappa_0}\mathbf{Q}_0. \tag{37}$$

This is the simplest explicit higher-order constitutive equations which neighbor upon the Navier–Stokes–Fourier equations in the limit of small deviation from local thermal equilibrium.

Another approximation can be applied to the constitutive relations (28) and (29). The third term of Eq. (29) can be approximated by an expression involving no gradient of $\mathbf{\Pi}$, $-\mathrm{Ec}\,\mathrm{Pr}(\mathbf{u}\cdot\nabla)\mathbf{u}\cdot\mathbf{\Pi}$, from the momentum equation of the conservation laws. It becomes $-(\mathbf{u}\cdot\nabla)(\mathbf{Q}+\mathrm{Ec}\,\mathrm{Pr}\mathbf{\Pi}\cdot\mathbf{u})$ when $-(\mathbf{u}\cdot\nabla)\mathbf{Q}$ is added, but then it can be neglected, together with $-(\mathbf{u}\cdot\nabla)\mathbf{\Pi}$ in (28), since they are purely convective terms. Also, it can be assumed that $(\mathbf{\Pi},\mathbf{Q})(\nabla\cdot\mathbf{u})$ are negligible in monatomic gas. We obtain the following algebraic form:

$$-2[\mathbf{\Pi}\cdot\nabla\mathbf{u}]^{(2)}-\frac{1}{N_\delta}\frac{p}{\eta}\{\mathbf{\Pi}q(N_\delta\kappa)+2\eta[\nabla\mathbf{u}]^{(2)}\}=0, \tag{38}$$

$$-\mathrm{Pr}\,\mathbf{\Pi}\cdot\nabla T-\mathbf{Q}\cdot\nabla\mathbf{u}-\frac{\mathrm{Pr}}{N_\delta}\frac{p}{\lambda/T}\{\mathbf{Q}q(N_\delta\kappa)+\lambda\nabla\ln T\}=0. \tag{39}$$

This set of nonlinear equations can be solved by iterative methods for given values of conserved variables and their derivatives. One difference between these and the original Eu relations[27] is the removal of a term $(\mathbf{u}\cdot\nabla)\mathbf{u}\cdot\mathbf{\Pi}$. By this, the new constitutive relations involve only p,T, and gradient of $\mathbf{u}$ and T.

Finally, with (21) and (26) the following constitutive relations will form a *thermodynamically consistent hydrodynamic computational model.*

$$\hat{\mathbf{\Pi}}q(c\hat{R})=\hat{\mathbf{\Pi}}_0+[\hat{\mathbf{\Pi}}\cdot\nabla\hat{\mathbf{u}}]^{(2)}, \tag{40}$$

$$\hat{\mathbf{Q}}q(c\hat{R})=\hat{\mathbf{Q}}_0+\hat{\mathbf{\Pi}}\cdot\hat{\mathbf{Q}}_0+\frac{1}{2\,\mathrm{Pr}}\hat{\mathbf{Q}}\cdot\nabla\hat{\mathbf{u}}, \tag{41}$$

where

$$\hat{\mathbf{\Pi}}\equiv\frac{N_\delta}{p}\mathbf{\Pi},\quad \hat{\mathbf{Q}}\equiv\frac{N_\delta}{p}\frac{\mathbf{Q}}{\sqrt{T/(2\epsilon)}},\quad \hat{R}^2=\hat{\mathbf{\Pi}}:\hat{\mathbf{\Pi}}+\hat{\mathbf{Q}}\cdot\hat{\mathbf{Q}},$$

$$\nabla\hat{\mathbf{u}} \equiv -2\eta\frac{N_\delta}{p}\nabla\mathbf{u}, \quad q(c\hat{R}) = \frac{\sinh(c\hat{R})}{c\hat{R}}.$$

C. Boundary condition

A close look of the constitutive equations, namely, (36)–(39), shows that they all share a unique property. As $N_\delta \to 0$, they all recover the Navier–Stokes–Fourier equations—the classical hydrodynamic equations. On the other hand, it is easy to deduce that they all also recover the Euler equations $\mathbf{\Pi}=\mathbf{Q}=0$ as $N_\delta \to \infty$. This rather unusual feature stems essentially from the presence of the nonlinear factor $q(N_\delta\kappa)$, which is indispensable for the constitutive equations to behave properly far from equilibrium. This feature is not shared by either the Burnett equations or other moment equations. The consequence of this capability by which they cover the two extreme regimes of density, that is, the rarefied and dense regimes of density, is that the slip phenomenon is naturally built in the generalized hydrodynamic equations.[28] Most of the previous hydrodynamic equations require some type of slip boundary conditions such as the Maxwell–Smoluchowski condition. However, it should be pointed out that the Maxwell–Smoluchowski condition, based on the notion of specular and diffuse reflections of gas molecules off the wall, was a temporary solution to a rather difficult nonlinear transport problem. It was developed to explain the slippage of the gas at the wall first observed by Kundt and Warburg (see Ref. 25, See 10.10). This condition requires some adjustable parameters in the form of accommodation coefficients and thus loses the predictability. According to the present equations, however, the notion of slip and temperature jump at the wall seems unnecessary. The nonslip boundary conditions are sufficient to treat high-Knudsen-number flows, provided that the nonlinear effect of entropy production is properly taken into account. This problem will be studied in Sec. V B.

In addition, the new hydrodynamic equations do not require any further condition beyond the Navier–Stokes nonslip boundary condition. Since the new constitutive relations involve only the first derivatives of velocity and temperature, they do not suffer the difficulty that often arises in other equations with higher-order derivative terms.[10]

III. GH-BURGERS' EQUATION

The constitutive relations (40) and (41) will provide the shear stress and heat flux for known conserved variables and their derivatives. But, it is not apparent how to solve them numerically and obtain their general properties. If a model system that closely duplicates the physical properties of the original equations is developed, it can serve as a very useful guide. Let us assume

$$\rho \approx 1, \quad Q_x = 0.$$

Then the conservation laws and the constitutive relation of shear stress can be approximated by

$$\frac{\partial u}{\partial t} + \frac{\partial}{\partial x}\left(\frac{u^2}{2} - \frac{u}{2}\right) + \frac{\partial}{\partial x}(u^2\hat{\Pi}) = 0, \tag{42}$$

$$\hat{\Pi}_0(\hat{\Pi}+1) - \hat{\Pi}q(\hat{\Pi}) = 0, \tag{43}$$

where

$$N_\delta = \frac{1}{\mathrm{Re}}, \quad \Pi_0 = -\eta\frac{\partial u}{\partial x}, \quad \kappa = \frac{\Pi}{u^2},$$

$$\hat{\Pi} \equiv N_\delta\kappa = N_\delta\frac{\Pi}{u^2}, \quad \eta = u.$$

Here $D\Pi/Dt$ is neglected by the adiabatic approximation. Let us call this the GH-Burgers' equation and denote its solution by $\hat{\Pi}_{\mathrm{GH}}$. Note that $\hat{\Pi}$ measures departure from the equilibrium in irreversible thermodynamics. If the kinematic term is neglected, the solution of Eq. (43) becomes

$$\hat{\Pi}_{\text{GH-I}} = \sinh^{-1}\hat{\Pi}_0. \tag{44}$$

If Eq. (43) is expanded in the series of N_δ, the Navier–Stokes, the second and third-order Burnett equations follow:

$$\hat{\Pi}_{\text{Navier–Stokes}} = \hat{\Pi}_0, \tag{45}$$

$$\hat{\Pi}_{\text{second Burnett}} = (1+\hat{\Pi}_0)\hat{\Pi}_0, \tag{46}$$

$$\hat{\Pi}_{\text{third Burnett}} = (1+\hat{\Pi}_0+\tfrac{5}{6}\hat{\Pi}_0^2)\hat{\Pi}_0. \tag{47}$$

It should be noted that Eq. (46) is the same as the simplified translational nonequilibrium model studied by Lumpkin *et al.* [Ref. 29, Eqs. 13(a) and 13(b)]. For completeness the conventional moment equation will be given by

$$\hat{\Pi}_{\mathrm{Grad}} = \frac{4\hat{\Pi}_0}{4-7\hat{\Pi}_0}, \tag{48}$$

from (Ref. 14, p. 268)

$$\Pi\frac{\partial u}{\partial x} + \frac{4}{3}(\Pi+u^2)\frac{\partial u}{\partial x} + \frac{u^2}{\eta}\Pi = 0.$$

Here the convective term $u\partial\Pi/\partial x$ has been ignored.

Except for Eq. (43), the constitutive equations are explicit in the Navier–Stokes stress $\hat{\Pi}_0$. Equation (43), which preserves the nonlinearity of the original equations (40) and (41), is highly nonlinear in nature so that its solution has to be calculated by iterative methods. Nevertheless, several basic properties can be easily proved:

(i) $\hat{\Pi}=0$ only when $\hat{\Pi}_0=0$;
(ii) the unique solution $\hat{\Pi}$ such that $\hat{\Pi}\hat{\Pi}_0>0$ exists for all $\hat{\Pi}_0$;
(iii) the curve $\hat{\Pi}(\hat{\Pi}_0)$ is tangent to the Navier–Stokes curve $(\hat{\Pi}=\hat{\Pi}_0)$ at $\hat{\Pi}_0=0$;
(iv) $\hat{\Pi}\to -1$ when $\hat{\Pi}_0=-\infty$, that is, always $\hat{\Pi}+1>0$;
(v) $d\hat{\Pi}/d\hat{\Pi}_0\to 0$ when $\hat{\Pi}_0=\pm\infty$.

Conditions (i) and (ii) mean one-to-one correspondence between the higher-order stress and the Navier–Stokes stress, which must be satisfied for all physical constitutive relations. Condition (iii) ensures the correct continuum asymptotic behavior, whereas conditions (iv) and (v) ensure

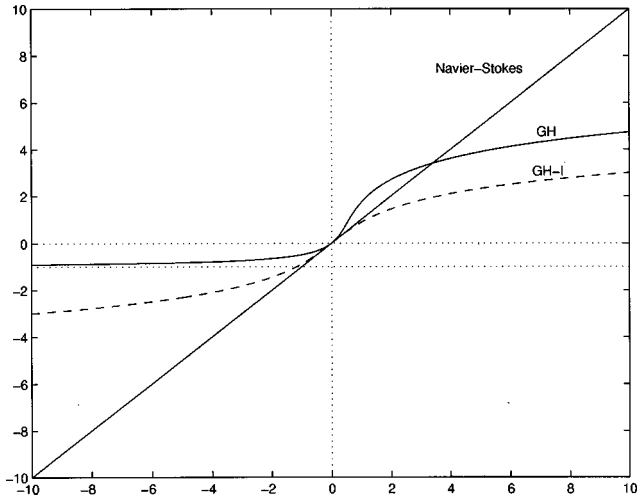

FIG. 1. Generalized hydrodynamic constitutive relations relative to the Navier–Stokes approximation. The axes represent the level of departure from equilibrium, $\hat{\Pi}$. The horizontal axis represents the linear approximation, $\hat{\Pi}_0$.

the correct free molecular limit. In particular, condition (iv) is equivalent to $\Pi_{xx}+p>0$ in the original constitutive equation, which is nothing but the free molecular limit. As mentioned in Sec. II C, this property confirms that the slip phenomenon at the solid boundary is built in the constitutive relations.

Five higher-order constitutive equations relative to the Navier–Stokes constitutive equations for the model problem are depicted in Figs. 1 and 2. From these figures, it becomes apparent that all other higher-order equations do not satisfy the correct free molecular limit and in some cases they even violate condition (ii) or (iii). In particular, there exists a singularity in Grad's constitutive equation. This may be responsible for the existence of a critical Mach number beyond which no continuous shock solution is possible, even though

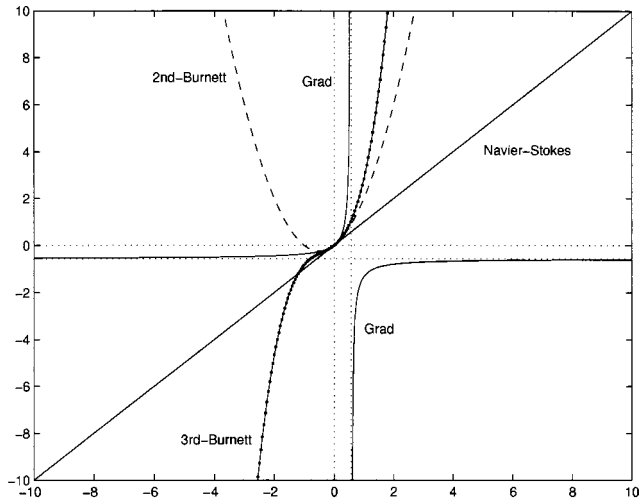

FIG. 2. Conventional higher-order hydrodynamic constitutive relations relative to the Navier–Stokes approximation. The axes represent the level of departure from equilibrium, $\hat{\Pi}$. The horizontal axis represents the linear approximation, $\hat{\Pi}_0$.

the critical Mach number may increase when higher-order moments are included.[17,21] Even though Grad's equation seems to satisfy the free molecular limit that might explain the slip phenomenon at the solid boundary, the limit value is not correct. On the other hand, the third-order Burnett equation satisfies conditions (i)–(iii), but does not satisfy conditions (iv) and (v). Consequently, the Burnett equations need some type of slip boundary condition. It is also interesting to note that conventional higher-order constitutive equations yield a larger stress in regimes far from equilibrium compared with the generalized hydrodynamic equations. As a result, the numerical algorithms based on the conventional relations become less effective since a large value of stress requires a smaller time step.

Therefore it can be summarized that most of the troubles observed in conventional constitutive equations are caused by the violation of some basic properties described earlier, in particular, conditions (ii) and (v). Furthermore, it can be demonstrated that some improvement of shock structure solutions by the Burnett equations and Grad's 13 moment method is not surprising if we examine regimes of positive stress in Figs. 1 and 2. Since the shock structure involves positive stress, the corresponding regimes in Figs. 1 and 2 are the first quadrant. For modest Mach numbers, they are restricted near small $\hat{\Pi}_0$. In these regimes, it is obvious that they approximate very closely the generalized hydrodynamic equation, namely, $\hat{\Pi}_{\mathrm{GH}}$. However, far from equilibrium they deviate drastically and could not recover the free molecular limit.

IV. COMPUTATIONAL METHODS

The generalized hydrodynamic equations (21) can be solved by modern numerical methods on hyperbolic conservation laws if $\mathbf{\Pi}$ and $\mathbf{Q}$ are calculated by (36) and (37) or (38) and (39). To illustrate numerical schemes for these equations let us consider the one-dimensional equations. In principle, the multidimensional problem can be solved by a one-dimensional numerical solver through the operator-splitting method. The one-dimensional GH equations in the conservative form can be written as the Euler equations plus a flux vector composed of the nonequilibrium components.

$$\frac{\partial \mathbf{u}}{\partial t}+\frac{\partial \mathbf{f}_T}{\partial x}=0, \tag{49}$$

where $\mathbf{u}$ is the solution vector of conserved variables, $\mathbf{f}_T$ represents the sum of the inviscid flux vector $\mathbf{f}$ and the flux vector of nonconserved variables $\mathbf{f}_v$. These vectors are given as

$$\mathbf{u}=\begin{pmatrix}\rho\\ \rho u\\ \rho v\\ \rho E\end{pmatrix},\quad \mathbf{f}=\begin{pmatrix}\rho u\\ \rho u^2+\dfrac{1}{N_\delta \mathrm{Re}}p\\ \rho u v\\ \left(\rho E+\dfrac{1}{N_\delta \mathrm{Re}}p\right)u\end{pmatrix},$$

$$\mathbf{f}_v=\frac{1}{\mathrm{Re}}\begin{pmatrix}0\\ \Pi_{xx}\\ \Pi_{xy}\\ \Pi_{xx}u+\Pi_{xy}v+\dfrac{1}{\mathrm{Ec\,Pr}}Q_x\end{pmatrix}. \tag{50}$$

This form of the generalized hydrodynamic equations is not different from the well-documented Navier–Stokes equations. Therefore, most of the modern high-resolution schemes, for instance, upwind schemes with Roe's Riemann solver,[30] can be applied without alteration. An example of such a scheme, the MUSCL-Hancock method,[31] can be described as follows. After a step involving a propagation over a time step $\Delta t/2$,

$$\overline{\mathbf{U}}_j=\mathbf{U}_j^n-\frac{\Delta t}{2\Delta x}(\mathbf{F}_{T,j+1/2}^n-\mathbf{F}_{T,j-1/2}^n), \tag{51}$$

where $\mathbf{F}_{T,j+1/2}=\mathbf{F}_{j+1/2}+\mathbf{F}_{v,j+1/2}$ and the inviscid numerical flux $\mathbf{F}$ can be given from an approximate Riemann solver, second-order extrapolations are introduced to $\overline{\mathbf{U}}$:

$$\mathbf{U}_{j+1/2}^l=\overline{\mathbf{U}}_j+\tfrac{1}{2}\underline{B}^l(\mathbf{U}_j^n-\mathbf{U}_{j-1}^n), \tag{52}$$

$$\mathbf{U}_{j-1/2}^r=\overline{\mathbf{U}}_j-\tfrac{1}{2}\underline{B}^r(\mathbf{U}_{j+1}^n-\mathbf{U}_j^n), \tag{53}$$

where

$$\underline{B}^{l,r}=\frac{1}{2}\left((1-\omega)B(b^{l,r})+(1+\omega)b^{l,r}B\left(\frac{1}{b^{l,r}}\right)\right),$$

$$b^l=\frac{1}{b^r}=\frac{\mathbf{U}_{j+1}^n-\mathbf{U}_j^n}{\mathbf{U}_j^n-\mathbf{U}_{j-1}^n},$$

and the ratios in the last equation are defined componentwise. The $\overline{\mathbf{U}}_j^n$ represents the average value of the conserved solution vector $\mathbf{u}$ in the jth cell at time level n. The Δt and Δx denote the time step and mesh width, respectively. An extrapolation parameter ω and a symmetric limiter $B(b)$ are introduced. Then the final scheme is

$$\mathbf{U}_j^{n+1}=\mathbf{U}_j^n-\frac{\Delta t}{\Delta x}(\overline{\mathbf{F}}_{T,j+1/2}-\overline{\mathbf{F}}_{T,j-1/2}), \tag{54}$$

where $\overline{\mathbf{F}}_{T,j+1/2}=\overline{\mathbf{F}}_{j+1/2}+\overline{\mathbf{F}}_{v,j+1/2}$ and $\overline{\mathbf{F}}_{j+1/2}=\mathbf{F}(\mathbf{U}_{j+1/2}^l,\mathbf{U}_{j+1/2}^r)$. With this numerical scheme on conserved variables, the only remaining problem is how to solve the highly nonlinear constitutive equations (40) and (41).

Let us first consider the GH-Burgers' equation (43). The requirements for an efficient iterative method are: (1) it must be extended to systems of nonlinear equations; (2) two initial guess values $\hat{\Pi}_0$ and $\hat{\Pi}_{\mathrm{GH\text{-}I}}$ have to be fully utilized. As methods that may satisfy such requirements, Newton's method and the method of iteration can be considered. However, it turned out that Newton's method is inadequate since the derivatives at the initial estimate $\hat{\Pi}_{\mathrm{GH\text{-}I}}$ are very small in most cases. As a result, the convergence is very slow and sometimes the iterations diverge. On the other hand, the method of iteration always provides converged solutions and takes only a few iterations, less than ten in most cases.

The method of iteration, which is of general applicability, uses the properties encoded in the equation itself by rearranging it into an equivalent expression of the form

$$\hat{\Pi}=g(\hat{\Pi})$$

such that if

$$f(\hat{\Pi}_{\mathrm{GH}})=0,\quad \hat{\Pi}_{\mathrm{GH}}=g(\hat{\Pi}_{\mathrm{GH}}).$$

Under suitable conditions, the algorithm

$$\hat{\Pi}_{n+1}=g(\hat{\Pi}_n),\quad n=1,2,3,...$$

will converge to a zero if $f(\hat{\Pi})=0$. The sufficient condition for the convergence is that $g(\hat{\Pi})$ and $g'(\hat{\Pi})$ are continuous on an interval about a root $\hat{\Pi}_{\mathrm{GH}}$, and $|g'(\hat{\Pi})|\leqslant 1$ for all $\hat{\Pi}$ in the interval.[32]

If Eq. (43) is rearranged into

$$\hat{\Pi}_{n+1}=\sinh^{-1}(\hat{\Pi}_0(1+\hat{\Pi}_n))\quad \text{for positive } \hat{\Pi}, \tag{55}$$

$$\hat{\Pi}_{n+1}=\frac{\hat{\Pi}_0}{q(\hat{\Pi}_n)-\hat{\Pi}_0}\quad \text{for negative } \hat{\Pi}, \tag{56}$$

then the sufficient condition for convergence can be proved by showing

$$\left|\frac{d}{d\hat{\Pi}}[\sinh^{-1}(\hat{\Pi}_0(1+\hat{\Pi}))]\right|<1\quad \text{for positive } \hat{\Pi}, \tag{57}$$

$$\left|\frac{d}{d\hat{\Pi}}\left[\frac{\hat{\Pi}_0}{q(\hat{\Pi})-\hat{\Pi}_0}\right]\right|<1\quad \text{for negative } \hat{\Pi}. \tag{58}$$

In this algorithm, $\hat{\Pi}_1=\hat{\Pi}_{\mathrm{GH\text{-}I}}$. The GH solutions obtained by this algorithm are depicted in Fig. 1.

A. One-dimensional shock structure ($\hat{u}_x$ and $\hat{Q}_x$)

Now let us consider the generalized equations (36), (37), (40), and (41) in the one-dimensional (1-D) shock structure problem. It can be easily shown that nonzero components are Π_{xx} and Q_x. Similar to the GH-Burgers' equations, they can be written as

$$\hat{\Pi}_{xx_{\mathrm{GH-I}}}=\frac{\sinh^{-1}(c\hat{R}_0)}{c\hat{R}_0}\hat{\Pi}_{xx_0}, \tag{59}$$

$$\hat{Q}_{x_{\mathrm{GH\text{-}I}}}=\frac{\sinh^{-1}(c\hat{R}_0)}{c\hat{R}_0}\hat{Q}_{x_0}, \tag{60}$$

and

$$\hat{\Pi}_{xx}q(c\hat{R})=(\hat{\Pi}_{xx}+1)\hat{\Pi}_{xx_0}(\equiv K_\Pi), \tag{61}$$

$$\hat{Q}_x q(c\hat{R})=(\hat{\Pi}_{xx}+1)\hat{Q}_{x_0}+\frac{3}{4\,\mathrm{Pr}}\hat{Q}_x\hat{\Pi}_{xx_0}(\equiv K_Q), \tag{62}$$

where

$$\hat{R}^2=\tfrac{3}{2}\hat{\Pi}_{xx}^2+\hat{Q}_x^2.$$

The factor 3/2 in $\hat{R}$ originates from relations, $\hat{\Pi}_{yy}=\hat{\Pi}_{zz}=-\hat{\Pi}_{xx}/2$. Notice that $\hat{\Pi}_{xx}$ and $\hat{Q}_x$ measure the magnitude of the viscous stress and heat flux relative to the hydrostatic pressure. Since the equations are invariant under a transform $\hat{Q}_x \leftrightarrow -\hat{Q}_x$, we need to investigate only two cases satisfying $\hat{\Pi}_{xx}\hat{Q}_x>0$. It can be shown that the following two iterations always converge, since they belong to the type of (57) and (58); for positive $\hat{\Pi}_{xx}$ and $\hat{Q}_x$,

$$\hat{R}_{n+1}=\frac{1}{c}\sinh^{-1}\{c(\hat{\Pi}_{xx_n}K_{\Pi_n}+\hat{Q}_{x_n}K_{Q_n})/\hat{R}_n\},$$
$$\frac{\hat{Q}_{x_{n+1}}}{\hat{\Pi}_{xx_{n+1}}}=\frac{K_{Q_n}}{K_{\Pi_n}}, \tag{63}$$

and for negative $\hat{\Pi}_{xx}$ and $\hat{Q}_x$,

$$\hat{\Pi}_{xx_{n+1}}=\frac{\hat{\Pi}_{xx_0}}{q(c\hat{R}_n)-\hat{\Pi}_{xx_0}},$$
$$\hat{Q}_{x_{n+1}}=\frac{(\hat{\Pi}_{xx_n}+1)\hat{Q}_{x_0}}{q(c\hat{R}_n)-3\hat{\Pi}_{xx_0}/4\,\mathrm{Pr}}, \tag{64}$$

where $\hat{\Pi}_{xx_1}$ and $\hat{Q}_{x_1}$ are given by Eqs. (59) and (60). This solution will be denoted by $\hat{\Pi}_{xx_{\mathrm{GH}}}$ and $\hat{Q}_{x_{\mathrm{GH}}}$.

B. 1-D shear flow problem ($\hat{v}_x$ only)

When only $\hat{v}_x$ exists, the constitutive relations become

$$\hat{\Pi}_{xy_{\text{GH-I}}}=\frac{\sinh^{-1}(c\hat{R}_0)}{c\hat{R}_0}\hat{\Pi}_{xy_0}, \tag{65}$$

$$\hat{\Pi}_{xx_{\text{GH-I}}}=Q_{x_{\text{GH-I}}}=0, \tag{66}$$

and

$$\hat{\Pi}_{xx}q(c\hat{R})=-\tfrac{2}{3}\hat{\Pi}_{xy}\hat{\Pi}_{xy_0}, \tag{67}$$

$$\hat{\Pi}_{xy}q(c\hat{R})=(\hat{\Pi}_{xx}+1)\hat{\Pi}_{xy_0}, \tag{68}$$

where

$$\hat{R}^2=3\hat{\Pi}_{xx}(\hat{\Pi}_{xx}-1).$$

Equations (67) and (68) become an equation of one variable $\hat{\Pi}_{xx}$,

$$\hat{\Pi}_{xx}q^2(c\hat{R})=-\tfrac{2}{3}(1+\hat{\Pi}_{xx})\hat{\Pi}_{xy_0}^2, \tag{69}$$

with a stress ellipse

$$\hat{\Pi}_{xy}=\mathrm{sign}(\hat{\Pi}_{xy_0})[-\tfrac{3}{2}(1+\hat{\Pi}_{xx})\hat{\Pi}_{xx}]^{1/2}. \tag{70}$$

The $\hat{\Pi}_{xx}$ can be obtained for a given $\hat{\Pi}_{xy_0}$ through

$$\hat{\Pi}_{xx_{n+1}}=-\frac{\hat{\Pi}_{xy_0}^2}{3q^2(c\hat{R}_n)/2+\hat{\Pi}_{xy_0}^2}. \tag{71}$$

It turned out that converged solutions were always obtained within a few iterations, less than ten for the tolerance value 10^{-5} in most cases, meaning that the iterations are absolutely converging and their computational cost is trivial.

V. APPLICATIONS: SHOCK STRUCTURE AND SLIP FLOW

A. Shock structure problem

The normal shock relations for a perfect gas are

$$\frac{\rho_2}{\rho_1}=\frac{u_1}{u_2}=\frac{(\gamma+1)M_1^2}{(\gamma-1)M_1^2+2}, \tag{72}$$

$$\frac{p_2}{p_1}=1+\frac{2\gamma}{\gamma+1}(M_1^2-1), \tag{73}$$

where the subscripts 1 and 2 represent the upstream and downstream states, respectively.

Since there is no solid boundary, the parameters Ec and ϵ can be simplified to

$$\mathrm{Ec}=(\gamma-1)M^2, \quad \epsilon=\frac{1}{\mathrm{Ec\,Pr}}. \tag{74}$$

For given Pr and γ a steady-state shock structure can be determined when three conserved variables (ρ_1,u_1,p_1) and Mach number M_1 at upstream state are specified. If the spatial coordinate is reduced by the mean free path l at the upstream condition, which can be given by $l=(\pi/2)^{1/2}\eta_1(RT_1)^{-1/2}/\rho_1$, the dimensionless parameters become

$$\mathrm{Kn}=1, \quad \mathrm{Re}=\sqrt{\frac{\gamma\pi}{2}}M_1, \quad N_\delta=\sqrt{\frac{2\gamma}{\pi}}M_1.$$

It should be mentioned that in general

$$l=\frac{m}{\sqrt{2}\pi d_1^2\rho_1}=\frac{2\sqrt{2}c^2}{\pi}\frac{\eta_1}{\rho_1\sqrt{RT_1}}$$

and thus the actual mean free path of molecules will be somewhat different.

Energy dissipation experiences a rapid change across the shock wave. A measure of such change can be defined if we introduce the calortropy production.[25] The calortropy production, which measures the energy dissipation in the system, is given by

$$\sigma_{\mathrm{cal}}=k_{\mathrm{B}}G\kappa\sinh\kappa. \tag{75}$$

A reduced calortropy production based on the upstream state can be defined by

$$\sigma_{\mathrm{cal}}^*\equiv\frac{\sigma_{\mathrm{cal}}}{k_{\mathrm{B}}G(n_1,T_1)}=\frac{c\hat{R}\sinh(c\hat{R})}{\rho^2}. \tag{76}$$

For comparison of various results of shock structure, the following parameters are very useful. The inverse of the

shock density thickness, and the shock temperature–density separation, which measures the separation between density and temperature profiles, are defined as

$$\frac{1}{\delta_s}=\left|\frac{d\overline{\rho}}{dx}\right|_{\max}\Big/\ (\overline{\rho}_2-\overline{\rho}_1), \tag{77}$$

$$\Delta_s=[x(\overline{\rho}=0.5)-x(\overline{T}=0.5)], \tag{78}$$

where $\overline{\rho}$ and $\overline{T}$ are the normalized density and temperature profile, e.g., $\overline{\rho}\equiv(\rho-\rho_1)/(\rho_2-\rho_1)$.

The previous results of these parameters in shock structure problem can be found in the works by Fiscko and Chapman,[33] Pham-Van-Diep *et al.*,[34] Balakrishnan *et al.*,[35] and Al-Ghoul and Eu.[27] It should be mentioned that the present calculation is based on a system of partial differential equations. Therefore it can be readily applied to two- and three-dimensional calculations for real configuration. The present solutions are obtained by the MUSCL-Hancock scheme with Roe's approximate Riemann solver and are proved to be numerically stable. The converged solutions are obtained for all gases ($\nu=5,9,\infty$) and Mach numbers (1–30) examined. Only the results of the Maxwellian molecule are presented since other molecules yield the qualitatively same results. The steady-state solution of the equations is obtained by marching forward in time from a set of initial conditions until the change in the solution is less than some prescribed value. A steady-state solution was considered to be obtained when the rms norm for the density dropped below 10^{-7}. In the shock structure problem a numerical boundary condition must be specified at the upstream and downstream boundaries of the computational domain. At the upstream boundary all the Euler characteristics are incoming for supersonic flow and therefore the variables can be specified by using the upstream initial condition. On the other hand, at the subsonic downstream boundary only one characteristic is incoming and thus one physical condition must be imposed. In the present study the velocity as predicted by Eq. (72) is specified. Other variables are extrapolated by using the interior values. In all cases a grid of 400 points with $\Delta x=0.5$ and the Courant–Friedrichs–Lewy (CFL) number 0.5 are used. For the second-order scheme one-sided extrapolation $\omega=-1$ and Minmod limiter $B(b)=\max[0,\min(1,b)]$ are used. In the method of iterations for the constitutive equations the solutions are considered converged when $|\hat{R}_{n+1}-\hat{R}_n|$ becomes smaller than the maximum tolerance value 10^{-5}.

To obtain stable numerical solutions the time step must be restricted by the CFL stability condition. For the generalized hydrodynamic equations it turns out that the following Navier–Stokes stability condition for upwind schemes works well:

$$\Delta t_{\rm NS}=\mathrm{CFL}\cdot\min(\Delta t_1,\Delta t_2), \tag{79}$$

where

$$\Delta t_1\equiv\frac{\Delta x}{|a|}+\frac{2\,\eta_{\rm NS}}{\rho a^2},\quad \Delta t_2\equiv\left[\frac{|a|}{\Delta x}+\frac{\eta_{\rm NS}}{\rho\Delta x^2}\right]^{-1}.$$

There exists a reason for such a property. From Fig. 1 it can be shown that $(\Delta t_1)_{\rm NS}$ or $(\Delta t_2)_{\rm NS}$ are always minimum except for $(\Delta t_2)_{\rm GH}<(\Delta t_2)_{\rm NS}$ when $0<\hat{\Pi}_0<\hat{\Pi}_0^*$. Here $\hat{\Pi}_0^*$ represents a nonzero value where $\hat{\Pi}_{\rm GH}=\hat{\Pi}_0$. Therefore the Navier–Stokes criterion (79) with CFL=0.5 will satisfy the time step restriction since

$$\left(\frac{\hat{\Pi}_{\rm GH}}{\hat{\Pi}_0}\right)_{\max}=1.7644\quad\text{at}\ \hat{\Pi}_0=0.79548.$$

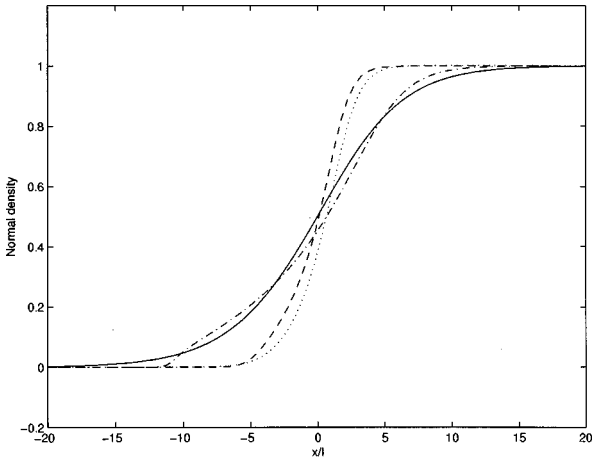

FIG. 3. Shock profiles for density for a Maxwellian gas. Solid line: $M=1.25$, dotted line: $M=2$, dashed line: $M=5$, dash-dotted line: $M=15$.

In Figs. 3–9 various aspects of hypersonic shock structure in a Maxwellian gas are illustrated. In Figs. 3–7 density, stress, heat flux, and calortropy production of a Maxwellian gas in generalized hydrodynamics (GH) are plotted for various Mach numbers. The shock profiles are in strong agreement with Eu's results based on a system of ordinary differential equations,[27] even though a minor difference exists in shock front for very high Mach numbers. It may be associated with numerical trouble which is often found in the region of high gradient. Nevertheless, the trend of the inverse shock density thickness is the same as Eu's exact result. Since Eu's theoretical calculation of argon gas ($\nu=9$) was

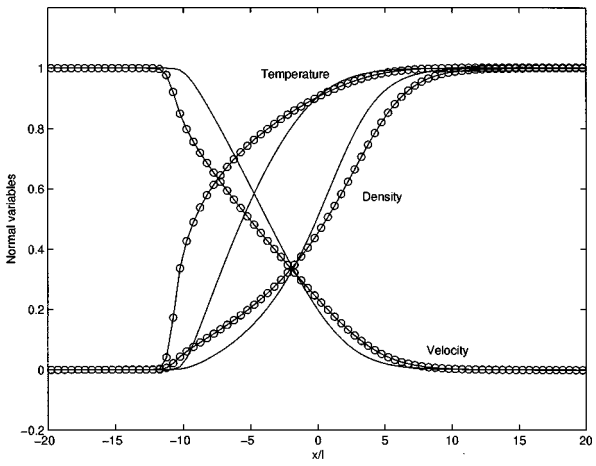

FIG. 4. Mach 15 shock profiles for a Maxwellian gas. Solid line with circle: generalized hydrodynamics, solid line: Navier–Stokes.

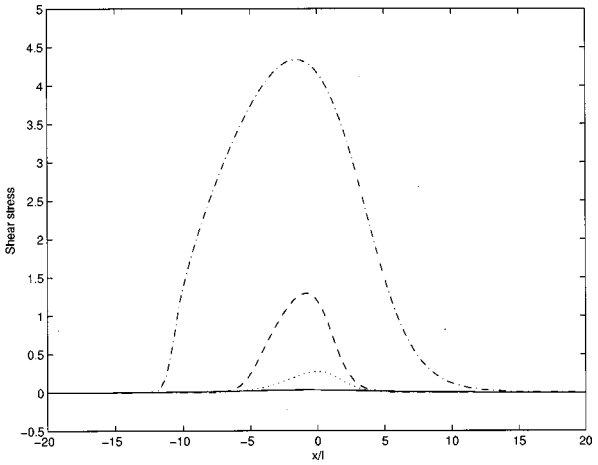

FIG. 5. Shock profiles for stress for a Maxwellian gas. The same meanings for the lines as in Fig. 3. The cases for $M=1.25$ is invisible in the present scale.

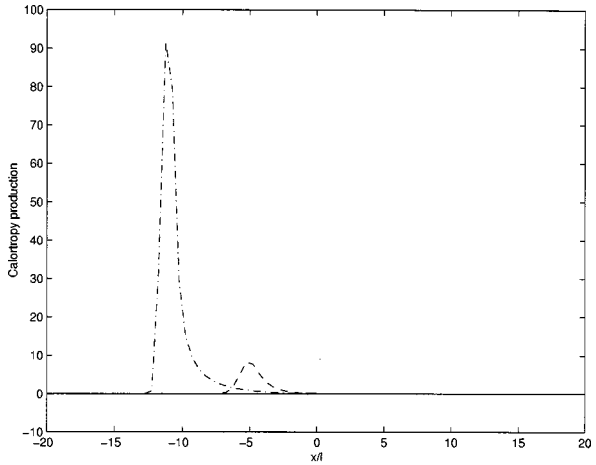

FIG. 7. Profiles for reduced calortropy production for a Maxwellian gas. The same meanings for the lines as in Fig. 3. The cases for $M=1.25$ and 2 are invisible in the present scale.

shown to agree very closely with experimental data, the present calculation based on a system of partial differential equations will also agree with experimental data. In fact, it can be observed in Figs. 3–9 that the present computational models predict shock structure in better agreement with DSMC results than the Navier–Stokes equations do. Another finding is that GH-I produces no better result than the Navier–Stokes–Fourier equations. This suggests that the coupling between the shear stress and velocity gradient cannot be ignored in highly nonequilibrium state.

In Fig. 10, in order to examine the effect of the nonlinear constitutive relations on the shock structure the level of departure from equilibrium is depicted with respect to the linear approximation. In the high Mach number regime ($M=15$), some parts of the shock structure involve a very large deviation and follow nonlinear relations different from the linear approximation. Two points that seem to be apart from the majority of circles represent the part very close to the upstream state. Note that the actual trend is very similar to one of the GH-Burgers' equation depicted in Fig. 1.

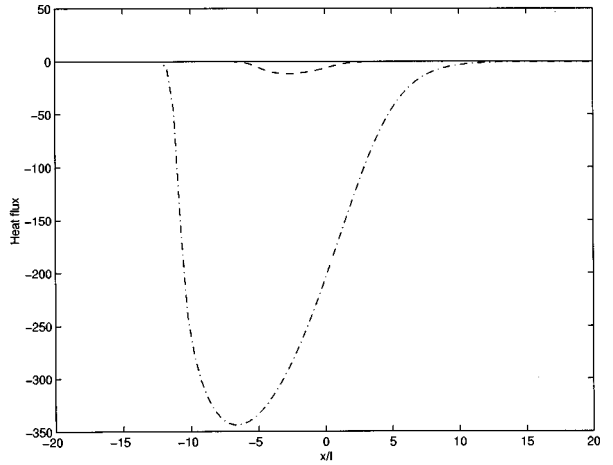

FIG. 6. Shock profiles for heat flux for a Maxwellian gas. The same meanings for the lines as in Fig. 3. The cases for $M=1.25$ and 2 are invisible in the present scale.

B. Slip flow problem

The slip-velocity phenomenon was first observed in 1875 by Kundt and Warburg in their experiment of low density gas flows. Since then, it remains as an intriguing problem in fluid dynamics because the conventional continuum equations cease to be valid and require the slip boundary condition. In order to investigate how the generalized equations describe the slip phenomenon, we will examine the constitutive relations under the gradient of shear velocity only, which are given in Sec. IV B. The first investigation of the generalized equations was done by Khayat and Eu.[36] They considered the cylindrical Couette flow of Lennard-Jones fluids for the purpose of explaining normal-stress effects and velocity slips. In the present work a one-dimensional planar problem is considered, but nevertheless it can manifest the essential element of the velocity-slip phenomenon. There exists no heat flux in the constitutive relations under the velocity-gradient only, whereas nonzero stresses should satisfy a stress ellipse (70). This constraint on the normal ($\hat{\Pi}_{xx}$) and shear ($\hat{\Pi}_{xy}$) stresses has a deep physi-

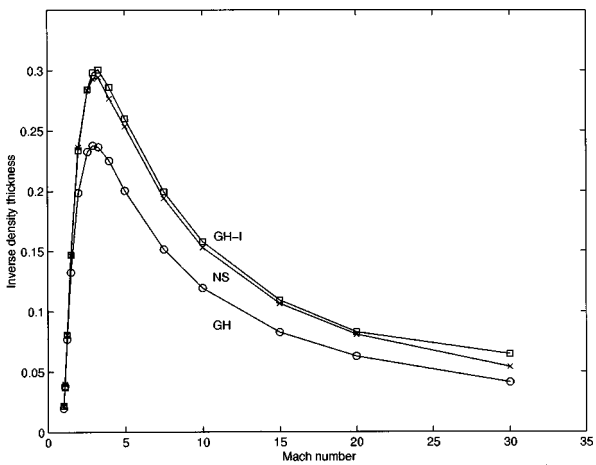

FIG. 8. Inverse shock density thickness for a Maxwellian gas. Circle: GH, × symbol: Navier–Stokes, square: GH-I.

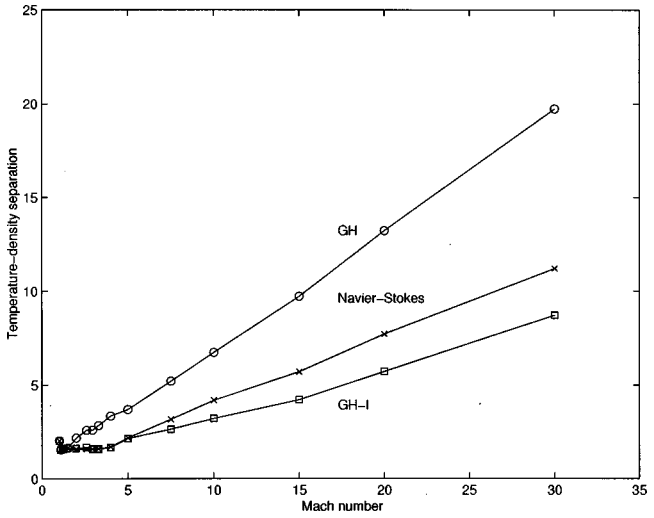

FIG. 9. Shock temperature–density separation for a Maxwellian gas. Circle: GH, × symbol: Navier–Stokes, square: GH-I.

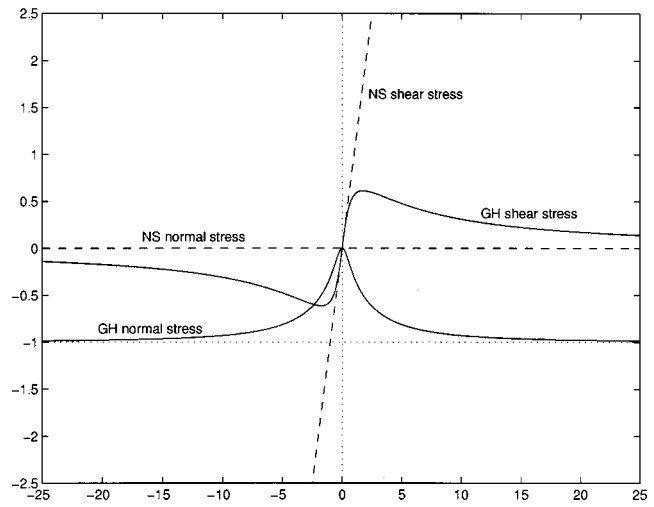

FIG. 11. The normal and shear stresses generated by v_x. The normal ($\hat{\Pi}_{xx}$) and shear ($\hat{\Pi}_{xy}$) stresses are plotted. The horizontal axis represents the velocity gradient ($\hat{v}_x$).

cal meaning. It requires that normal and shear stresses should be confined to the stress ellipse, and consequently ($\hat{\Pi}_{xx}+1$) and $\hat{\Pi}_{xy}$ approach zero as the velocity-gradient increases. This unusual feature is described in Fig. 11. Note that the shear stress $\hat{\Pi}_{xy}$ becomes maximum at

$$|\hat{\Pi}_{xy_0}|=\frac{\sqrt{6}}{2}q\left(\frac{3}{2}c\right) \quad \text{or} \quad |v_x|=\sqrt{6}q\left(\frac{3}{2}c\right)\frac{p}{N_\delta}. \tag{80}$$

Here $\sqrt{6}q(3c/2)=3.5089$ for a Maxwellian molecule. The ultimate role of this asymptotic behavior is that the gas slips near the solid wall. As a result, the velocity-slip phenomenon, which has nothing to do with surface–gas molecular interaction, can be explained in purely hydrodynamical terms.

This finding can be confirmed by a numerical simulation of the GH equations for a simple geometry. The planar Couette flow, the steady relative motion of two parallel surfaces that are separated by a gas, can serve as a test case. Consider the flow of a gas between infinite parallel plates, the left plate moving at velocity $-v_0$ and the right one moving at velocity v_0. In this geometry, all properties can be assumed to vary only with a coordinate x. The boundary conditions can be given:

$$\text{At } x=-D/2: \quad v=-v_0, \quad T=T_w, \quad \frac{\partial p}{\partial x}=0, \tag{81}$$

$$\text{At } x=D/2: \quad v=v_0, \quad T=T_w, \quad \frac{\partial p}{\partial x}=0, \tag{82}$$

where D is a gap between two plates. The conservation laws (49) and (50) are solved in the same way as the shock-structure problem. The constitutive equations of $\hat{\Pi}_{xx}$, $\hat{\Pi}_{xy}$, and $\hat{Q}_x$ are solved by incorporating two solvers, one given in (61) and (62), and another given in (69) and (70). The flow is computed for a Mach number ($M=0.99$) with a grid of 100 points. The gas is assumed to be Maxwellian. The initial conditions ($u=v=0, p=T=1$) and boundary conditions ($v_0=1, T_w=1$) are chosen to obtain the steady-state solutions. In particular, the sum of initial density is maintained unchanged since the mass of the gas between the two plates will be conserved in time. In order to avoid possible contamination of solutions by high-order boundary conditions, the first-order accuracy was maintained throughout the computational domain. In Fig. 12 the reduced velocity at the plate $(v_0-v)/v_0$ is plotted versus the Knudsen number in logarithmic scale. The velocity v is defined at the center of the nearest cell to the wall. The slip starts at the critical Knudsen number 0.285 and rises rapidly, reaching full slip eventually in high Knudsen number regime. This result coincides with the theoretical prediction and is caused by the presence of the normal stress $\hat{\Pi}_{xx}$. Compare with the Navier–Stokes equations in which the normal stress cannot be generated by v_x.

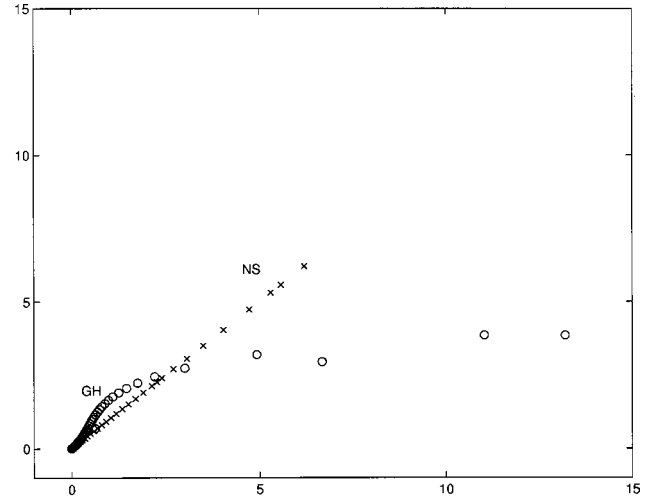

FIG. 10. The level of departure from thermodynamic equilibrium in shock structure problem (Mach number 15). The axes represent the level of non-equilibrium, $\hat{R}$. The horizontal axis represents the linear approximation, $\hat{R}_0$. Compare with Fig. 1.

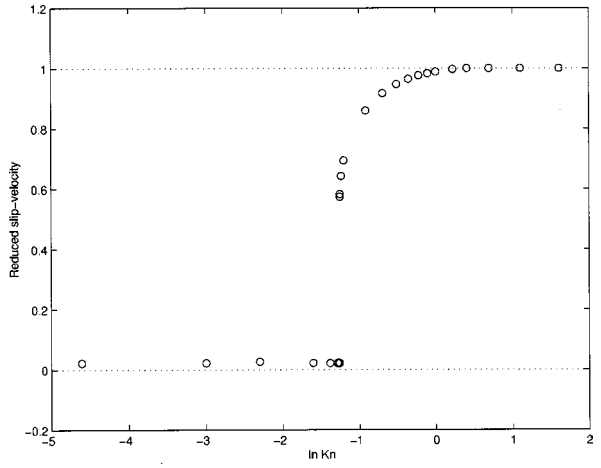

FIG. 12. The velocity slip $((v_0-v)/v_0)$ in plane Couette flow is plotted for various values of Kn in logarithmic scale.

VI. RAREFIED GAS DYNAMICS AND MICROSCALE FLOW

Previously, rarefied gas flow encountered in hypersonic flight was considered a primary problem in the study of high-Knudsen-number flows. There is a very large body of literature on this problem.[1] In order to examine how the generalized hydrodynamic equations can be applied to this problem, let us consider a typical case, for example, a hypersonic vehicle at an altitude of 93 km. For realistic values of flight conditions ($L=1$ m, $u_\infty=8$ km/s), dimensionless parameters can be approximated as

$$\mathrm{Re}=1151, \quad M=28.7, \quad \mathrm{Kn}=0.037, \quad N_\delta=1.$$

For this range of parameters, each term in the constitutive relations (38) and (39) is important, so that all terms should be retained. In fact, this is the case for which the hypersonic shock structure problem was solved in Sec. V. In the hypersonic shock structure problem ($M=30$) the parameters (Kn and N_δ) are larger than those in the hypersonic flight. Therefore, the computational model used in Sec. V can be applied directly to rarefied flow in a hypersonic flight condition.

Recently it has become important to develop an engineering tool for designing MEMS.[37] In contrast to rarefied gas dynamics, the microscale flows involve a relatively high density and a low velocity. As a result, DSMC, which has been highly successful in rarefied hypersonic flow, becomes less effective owing to the increase of the number of particles. However, it seems that the present computational models do not suffer such difficulty. Let us consider a microchannel with helium gas at standard temperature, and pressure condition. For a practical problem ($L=1.2\,\mu$m, $u_\infty=20$ cm/s), dimensionless parameters can be approximated as

$$\mathrm{Re}=2.3\times10^{-3}, \quad M=2.06\times10^{-4},$$

$$\mathrm{Kn}=0.145, \quad N_\delta=3.08\times10^{-5}.$$

For these parameters (creeping microflow), the terms associated with no N_δ^{-1} can be neglected and the resulting constitutive relations are precisely the Navier–Stokes–Fourier equations (32) and (33). In addition, it can be found from Eq. (21) that the hydrostatic pressure is the dominant term in the conservation laws. The very small value of N_δ may imply that the slip-velocity arising from the pure hydrodynamic origin is negligible. This may in turn suggest that the slip-velocity in microscale flows is caused largely by the gas-surface molecular interaction that is dependent upon the pressure.

VII. DISCUSSION AND CONCLUSION

As a step toward developing thermodynamically consistent multidimensional computational models for high-Knudsen-number flows, Eu's generalized hydrodynamic equations have been considered in the present paper. As a result, a form of the governing equations suitable for modern high resolution multidimensional numerical schemes is obtained. The main advantage of this form is that with a proper subroutine of constitutive relations numerical implementation does not require any further work beyond the Navier–Stokes codes. On the basis of this new development, the general properties of conventional computational models, namely, the Burnett and Grad's equations, are clearly shown. The new formulation is applied to the hypersonic shock structure and slip flow problems. It is proved numerically that the new computational models yield shock structures over the entire range of Mach numbers and for all gases. Even though the present study is restricted to the one-dimensional situation, there is no theoretical barrier for the multidimensional extension, inasmuch as the one-dimensional Riemann solver is directly extendible to a multidimensional problem.

Nevertheless, extension to multidimensional problems presents some numerical challenges. Solving the constitutive equations may cost a considerable amount of computing time compared with a one-dimensional problem. However, if a method in which the constitutive relations are stored as a separate database or an operator-splitting method is adopted, the additional computational cost can be trivial compared with the Navier–Stokes relations. The numerical solutions using multidimensional computational models will be reported in a forthcoming paper.[38]

The present computational models are based on Eu's generalized hydrodynamic equations which have been derived for dilute gases. This fact may imply that the models cannot be applied to other gases. However, as shown by Eu,[26] the same form of the governing equations holds for dense gases and therefore the essence of the present work can go over to dense gases.

Finally, it is worthwhile mentioning a reason behind the success of the present computational models. In the previous methods, the main concern was to raise the order of approximations to the actual distribution function. As a result, the evolution equations involve many higher-order terms. However, it should be pointed out that although those terms are mathematically definable, they do not have important physical meanings, except for the stress and heat flux. Therefore, it is not surprising that the computation of some higher-order moments equations makes not only the problem complicated,

but also yields the solutions that fall short of the desired aim. This finding implies that more accurate approximations to the distribution function are needed. Such approximations were indeed developed by Eu,[24] who found the nonequilibrium canonical distribution function by developing the cumulant expansion of the collision integral. His theory turned out to fulfill the requirement that the most important role of higher-order terms is to increase the entropy, so that the second law of thermodynamics must be taken into account in all approximations. The present study confirms the fundamental importance of exploiting the laws of thermodynamics in the study of high-Knudsen-number flow.

ACKNOWLEDGMENTS

This work was performed while the author held a National Research Council (NASA Goddard) Research Associateship. He wishes to express his deep appreciation to Professor B. C. Eu of McGill University for his encouragement and valuable advice.

APPENDIX A: NONEQUILIBRIUM CANONICAL DISTRIBUTION FUNCTION

According to Eu's theory[25] the nonequilibrium canonical form can be expressed in the exponential form

$$f_i = \exp[-\beta(H_i + H_i^{(1)} - \mu_i)], \tag{A1}$$

where

$$H_i = \tfrac{1}{2} m_i c_i^2 + m_i \Psi_i(r), \tag{A2}$$

$$H_i^{(1)} = \sum_{\alpha \geqslant 1} X_{\alpha i} h_{\alpha i}, \tag{A3}$$

and μ_i is the normalization factor

$$\exp(-\beta \mu_i) = \langle \exp[-\beta(H_i + H_i^{(1)})] \rangle / n_i. \tag{A4}$$

c_i is the peculiar velocity of particle i defined by $c_i = \mathbf{v} - \mathbf{u}$, where $\mathbf{v}$ and $\mathbf{u}$ are the particle velocity and the average bulk velocity, respectively. n_i is the number density, Ψ_i is the potential energy density, and $h_{\alpha i}$ represent stress tensor, excess stress, heat flux, diffusion flux, etc. The angular brackets $\langle\ \rangle$ denotes integration in the particle velocity. The $X_{\alpha i}$ do not depend on the particle velocity, but are functions of macroscopic variables such as ρ_i, $\mathbf{u}$, E, and $\mathbf{\Pi}$, $\mathbf{Q}$, etc. Thus they occupy a role similar to the coefficients $A_i^{(1)}, A_i^{(2)}$, etc., in the Chapman–Enskog expansion series,

$$f_i = f_i^{(0)}[1 + A_i^{(1)} c_i + A_i^{(2)} : [m_i c_i c_i]^{(2)} + \cdots], \tag{A5}$$

where $f_i^{(0)}$ represents the Maxwell–Boltzmann distribution function and $A_i^{(1)} = 0, A_i^{(2)} = (m_i / 2 k_B T) \mathbf{\Pi}_i / \rho_i$. However, unlike the Maxwell–Grad moment method, $X_{\alpha i}$ are not predetermined in terms of macroscopic variables. They are determined through careful consideration of the entropy production. For example, X_{1i} has approximately the form of $-\mathbf{\Pi}_i / (2 p_i)$. In fact, this is very crucial in not leaving out the entropy in the solution method for the Boltzmann equation. On the contrary, the entropy plays no role in determining the coefficients of the distribution function in other moment methods and consequently is completely left out in the development despite its fundamental importance. This remarkable feature in generalized hydrodynamics stems from the fact that the distribution is not approximate and, even if an approximate $H_i^{(1)}$ were taken, it leads to the positivity of the entropy production.

The new constitutive relations (22) and (23) bear traces of the nonequilibrium canonical form. It is a nonlinear factor $q(N_\delta \kappa)$ found in the last terms. This factor is related to the cumulant approximation for the entropy production and appears as a common factor when the dissipation terms are calculated in terms of $X_{\alpha i}$.

APPENDIX B: EU'S CLOSURE

In Eq. (27), the higher-order moments ψ_2 and ψ_3 are assumed to be zero. This closure is different from the common practice in the moment method where higher-order moments are expressed in terms of lower-order moments. However, it should be kept in mind that Grad's closure yields the most symmetric closure in a mathematical sense, but there is no theoretical justification for it. Therefore, setting higher-order terms simply to zero can be a viable option, apart from its simplicity. The reason is that Eu's closure has the same meaning of taking only measurable observables. Those not observable can be neglected on the ground that they should not be expressed in terms of the observables. In fact, if we define another form of moment

$$\Theta_k = \langle H^{(k)}(\sqrt{m/(k_B T)}\,\mathbf{c}) f(\mathbf{c}, t) \rangle, \tag{B1}$$

it can be shown that Eu's closure (27) is equivalent to[25,27]

$$\Theta_3 = -\Theta_1 \delta = 0, \quad \Theta_4 = -\Theta_2 \delta = -\mathbf{\Pi} \delta. \tag{B2}$$

As in Grad's closure, the higher-order terms are expressed in lower-order terms. The only difference is how to implement the same idea.

APPENDIX C: ALGEBRAIC EQUATIONS FOR POWERS OF N_δ

Let us examine the generalized hydrodynamic equations. The main concern is to see the differences between the new equations and the conventional equations. Expand $\mathbf{\Pi}$, $\mathbf{Q}$, and $q(N_\delta \kappa)$ in series of N_δ,

$$\mathbf{\Pi} = \mathbf{\Pi}_0 + N_\delta \mathbf{\Pi}_1 + N_\delta^2 \mathbf{\Pi}_2 + \cdots, \tag{C1}$$

$$\mathbf{Q} = \mathbf{Q}_0 + N_\delta \mathbf{Q}_1 + N_\delta^2 \mathbf{Q}_2 + \cdots, \tag{C2}$$

$$q(N_\delta \kappa) = 1 + \frac{1}{3!} \kappa_0^2 N_\delta^2 + \frac{1}{5!} \kappa_0^4 N_\delta^4 + \cdots. \tag{C3}$$

Then the constitutive relations (38) and (39) produce a hierarchy of algebraic equations for powers of N_δ,

$$\mathbf{\Pi}_0 = -2 \eta [\nabla \mathbf{u}]^{(2)}, \tag{C4}$$

$$\mathbf{Q}_0 = -\lambda \nabla \ln T, \tag{C5}$$

$$\mathbf{\Pi}_1 = -\frac{2 \eta}{p} [\mathbf{\Pi}_0 \cdot \nabla \mathbf{u}]^{(2)}, \tag{C6}$$

$$\mathbf{Q}_1 = -\frac{\lambda / T}{p} \left\{ \mathbf{\Pi}_0 \cdot \nabla T + \frac{1}{\mathrm{Pr}} \mathbf{Q}_0 \cdot \nabla \mathbf{u} \right\}. \tag{C7}$$

The first two (zeroth order in N_δ) are nothing but the Navier–Stokes–Fourier equations and the next two (first order in N_δ) are equivalent to the second-order Burnett equations. Here it should be noted that the nonlinear factor $q(N_\delta \kappa)$ plays no role in this expansion since there is no linear order term. Therefore, it can be inferred that the second-order Burnett equation contains no further information of the entropy production in comparison with the Navier–Stokes–Fourier equations and consequently their use becomes questionable for the study of problems far from equilibrium. In fact, it was proved that the entropy production in the conventional Burnett equations is not guaranteed to remain positive for all values of velocity and temperature gradients.[11] On the other hand, this explains why the Navier–Stokes–Fourier approximation is so successful in regimes of small deviation from local thermodynamic equilibrium and sometimes applicable even in the regime beyond.

[1] M. S. Ivanov and S. F. Gimelshein, ''Computational hypersonic rarefied flows,'' Annu. Rev. Fluid Mech. **30**, 469 (1998).

[2] C. Kim, K. E. Goodson, M. Faghri, L. S. Yao, W. S. Chang, A. Gopinath, S. S. Sadhal, and E. H. Trinh, ''Microelectromechanical systems (MEMS),'' *Proceedings of the 1997 International Mechanical Engineering Congress and Exposition* (ASME, 1997), Vol. 62, Dallas.

[3] C. M. Ho and Y. C. Tai, ''Micro-electro-mechanical-systems (MEMS) and fluid flows,'' Annu. Rev. Fluid Mech. **30**, 579 (1998).

[4] G. A. Bird, *Molecular Gas Dynamics* (Clarendon, Oxford, 1976).

[5] E. S. Oran, C. K. Oh, and B. Z. Cybyk, ''Direct simulation Monte Carlo: Recent advances and applications,'' Annu. Rev. Fluid Mech. **30**, 403 (1998).

[6] R. P. Nance, D. B. Hash, and H. A. Hassan, ''Role of boundary conditions in Monte Carlo simulation of microelectromechanical systems,'' J. Spacecr. Rockets **12**, 447 (1998).

[7] S. Chapman and T. G. Cowling, *The Mathematical Theory of Non-uniform gases* (Cambridge University Press, New York, 1970).

[8] X. Zhong and G. H. Furumoto, ''Augmented Burnett-equation solutions over axisymmetric blunt bodies in hypersonic flow,'' J. Spacecr. Rockets **32**, 588 (1995).

[9] R. Balakrishnan and R. K. Agarwal, ''Numerical simulation of the BGK-Burnett equations for hypersonic blunt body flows using the kinetic wave-particle flux splitting algorithm,'' AIAA Paper No. 98-0848 (1998).

[10] C. J. Lee, ''Unique determination of solutions to the Burnett equations,'' AIAA J. **32**, 985 (1994).

[11] F. E. Lumpkin III, I. D. Boyd, and E. Venkatapathy, ''Comparison of continuum and particle simulations of expanding rarefied flows,'' AIAA Paper No. 93-0728 (1993).

[12] K. A. Comeaux, D. R. Chapman, and R. W. MacCormack, ''An analysis of the Burnett equations based on the second law of thermodynamics,'' AIAA Paper No. 95-0415 (1995).

[13] H. Grad, ''On the kinetic theory of rarefied gases,'' Commun. Pure Appl. Math. **2**, 331 (1949).

[14] H. Grad, ''The profile of a steady plane shock wave,'' Commun. Pure Appl. Math. **5**, 257 (1952).

[15] T. I. Gombosi, *Gaskinetic Theory* (Cambridge University Press, New York, 1994).

[16] L. H. Holway, ''Existence of kinetic theory solutions to the shock structure problem,'' Phys. Fluids **7**, 911 (1964).

[17] W. Weiss, ''Comments on 'Existence of kinetic theory solutions to the shock structure problem' [Phys. Fluids. **7**, 911 (1964)]'' Phys. Fluids **8**, 1689 (1996).

[18] C. D. Levermore, ''Moment closure hierarchies for kinetic theories,'' J. Stat. Phys. **83**, 1021 (1996).

[19] C. D. Levermore and W. J. Morokoff, ''The Gaussian moment closure for gas dynamics,'' SIAM (Soc. Ind. Appl. Math.) J. Appl. Math. **59**, 72 (1998).

[20] C. P. T. Groth, P. L. Roe, T. I. Gombosi, and S. L. Brown, ''On the nonstationary wave structure of a 35-moment closure for rarefied gas dynamics,'' AIAA Paper No. 95-2312 (1995).

[21] S. Brown, ''Approximate Riemann solvers for moment models of dilute gases,'' Ph.D. thesis, The University of Michigan, 1996.

[22] R. Roveda, D. B. Goldstein, and P. L. Varghese, ''Hybrid Euler/particle approach for continuum/rarefied flows,'' J. Spacecr. Rockets **35**, 258 (1998).

[23] I. Boyd, G. Chen, and G. Candler, ''Predicting failure of the continuum fluid equations in transitional hypersonic flows,'' Phys. Fluids **7**, 210 (1995).

[24] B. C. Eu, ''A modified moment method and irreversible thermodynamics,'' J. Chem. Phys. **73**, 2958 (1980).

[25] B. C. Eu, *Kinetic Theory and Irreversible Thermodynamics* (Wiley, New York, 1992).

[26] B. C. Eu, ''Non-equilibrium grand ensemble method for dense fluids,'' J. Chem. Phys. **107**, 222 (1997).

[27] M. Al-Ghoul and B. C. Eu, ''Generalized hydrodynamics and shock waves,'' Phys. Rev. E **56**, 2981 (1997).

[28] R. E. Khayat and B. C. Eu, ''Generalized hydrodynamics, normal-stress effects, and velocity slips in the cylindrical Couette flow of Lennard-Jones fluids,'' Phys. Rev. A **39**, 728 (1989).

[29] F. E. Lumpkin III, D. R. Chapman, and C. Park, ''A new rotational relaxation model for use in hypersonic computational fluid dynamics,'' AIAA Paper No. 89-1737 (1989).

[30] P. L. Roe, ''Approximate Riemann solvers, parameter vectors, and difference schemes,'' J. Comput. Phys. **43**, 357 (1981).

[31] B. van Leer, ''On the relation between the upwind-differencing schemes of Godunov, Enguist-Osher and Roe,'' SIAM (Soc. Ind. Appl. Math.) J. Sci. Stat. Comput. **5**, 1 (1985).

[32] C. F. Gerald and P. O. Wheatly, *Applied Numerical Analysis* (Addison–Wesley, Palo Alto, CA, 1983).

[33] K. A. Fiscko and D. R. Chapman, ''Comparison of Burnett, super-Burnett and Monte Carlo solutions for hypersonic shock structure,'' Prog. Astronaut. Aeronaut. **118**, 374 (1989).

[34] G. C. Pham-Van-Diep, D. A. Erwin, and E. P. Muntz, ''Testing continuum descriptions of low-Mach-number shock structure,'' J. Fluid Mech. **232**, 403 (1991).

[35] R. Balakrishnan, R. K. Agarwal, and K. Y. Yun, ''High-order distribution functions, BGK-Burnett equations and Boltzmann's H-theorem,'' AIAA Paper No. 97-2551 (1997).

[36] R. E. Khayat and B. C. Eu, ''Generalized hydrodynamics and Reynolds-number dependence of steady-flow properties in the cylindrical Couette flow of Lennard-Jones fluids,'' Phys. Rev. A **40**, 946 (1989).

[37] E. B. Arkilic, M. A. Schmidt, and K. S. Breuer, ''Gaseous slip flow in long microchannels,'' IEEE J. MEMS **6**, 167 (1997).

[38] R. S. Myong, ''A new hydrodynamic approach to computational hypersonic rarefied gasdynamics, '' AIAA Paper No. 99-3578 (1999).